Article

IR Spectroscopic Characterization of H_2 Adsorption on Cationic Cu_n^+ (n = 4−7) Clusters

Olga V. Lushchikova, Hossein Tahmasbi, Stijn Reijmer, Rik Platte, Jörg Meyer,* and Joost M. Bakker*

Read Online

ACCESS | 📊 Metrics & More | 📰 Article Recommendations | 🆘 Supporting Information

ABSTRACT: IR spectra of cationic copper clusters Cu_n^+ (n = 4−7) complexed with hydrogen molecules are recorded via IR multiple-photon dissociation (IRMPD) spectroscopy. To this end, the copper clusters are generated via laser ablation and reacted with H_2 and D_2 in a flow-tube-type reaction channel. The complexes formed are irradiated using IR light provided by the free-electron laser for intracavity experiments (FELICE). The spectra are interpreted by making use of isotope-induced shifts of the vibrational bands and by comparing them to density functional theory calculated spectra for candidate structures. The structural candidates have been obtained from global sampling with the minima hopping method, and spectra are calculated at the semilocal (PBE) and hybrid (PBE0) functional level. The highest-quality spectra have been recorded for $[5Cu, 2H/2D]^+$, and we find that the semilocal functional provides better agreement for the lowest-energy isomers. The interaction of hydrogen with the copper clusters strongly depends on their size. Binding energies are largest for Cu_5^+, which goes hand in hand with the observed predominantly dissociative adsorption. Due to smaller binding energies for dissociated H_2 and D_2 for Cu_4^+, also a significant amount of molecular adsorption is observed as to be expected according to the Evans−Polanyi principle. This is confirmed by transition-state calculations for Cu_4^+ and Cu_5^+, which show that hydrogen dissociation is not hindered by an endothermic reaction barrier for Cu_5^+ and by a slightly endothermic barrier for Cu_4^+. For Cu_6^+ and Cu_7^+, it was difficult to draw clear conclusions because the IR spectra could not be unambiguously assigned to structures.
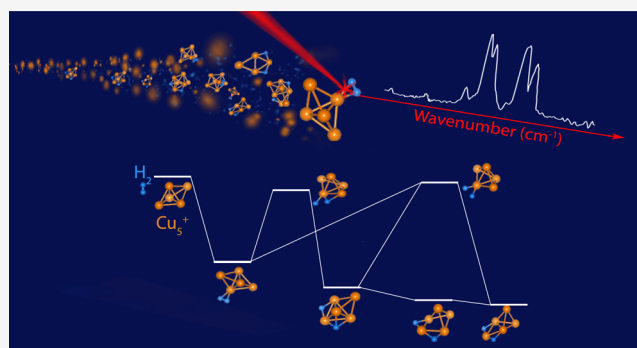
INTRODUCTION

The understanding of the adsorption of molecular hydrogen onto metals plays an important role in the development of various fields, such as metallurgy, hydrogen storage, and catalysis. Not only is H_2 itself considered as the cleanest and most efficient fuel since it does not produce any pollutants during combustion,[1] it is also a feedstock for the production of other renewable fuels. However, given the 4.5 eV bond energy, the activation of the H−H bond is often a difficult step. One important example is methanol production from syngas (H_2/CO_2/CO) in industry, where molecular hydrogen is dissociated over a $Cu/ZnO/Al_2O_3$ catalyst and the dissociation barrier is lowered to 0.7 eV.[2,3] The hydrogenation reaction still takes place at elevated temperatures (and pressures) to overcome this considerably reduced barrier.

As a simple model system for heterogeneous catalysis, the interaction and reactive dynamics of H_2 on low-index copper surfaces has been studied very extensively under well-defined surface science conditions. Molecular beam experiments have shown that reactive scattering only occurs if the incoming collision energy is sufficiently high.[4−6] In combination with theoretical work, it is therefore now well established that hydrogen is not activated at room temperature due to barriers

on the order of 0.5 eV.[7−10] Consequently, dissociative chemisorption of H_2 on ideal crystalline copper surfaces is quite well characterized and understood in detail, with only a few open questions in its theoretical description remaining.[11,12] However, the irregularly shaped surfaces of real-world industrial catalysts and their finite-sized catalytically active particles require other model systems, which can be provided by copper clusters.

Surprisingly, the interaction between copper clusters and H_2 has experimentally barely been studied, with two independent experiments reporting no H_2 adsorption onto neutral copper clusters at room temperature, both under single-collision and multicollision conditions.[13−15] For ionic species, only the reactions of the Cu^+ ion and the Cu_2^+ dimer with H_2 were reported,[16,17] yielding binding energies in good agreement with

the results from density functional theory (DFT) calculations. Binding of H_2 to the Cu^+ ion was interpreted to be a mix of donation to Cu^+ from the H_2 σ orbital, and back-donation from the Cu^+ $3d\pi$ orbitals to the H_2 σ^* antibonding orbital, weakening the H−H bond. Theoretically, the interaction between copper clusters and H_2 has been studied more intensively.[18−24] Cheng and co-workers systematically studied the growth of (neutral) Cu_n (n = 2−15) clusters and their reactions with H_2 and found that Cu_4 has the highest dissociative chemisorption energy and that it decreases gradually with increasing cluster size, flattening off after n = 12.[20−22] It was also revealed that the adsorption energy is lower for even-sized clusters.[19]

Regarding catalytically active clusters on an inert support material, López et al.[25] suggested that Cu clusters deposited on a SiO surface exhibit much higher reactivity toward dissociative adsorption of molecular hydrogen. For example, their calculations show that while the neutral Cu_5 cluster in the gas phase cannot dissociate H_2, after the deposition on the SiO support it becomes an active catalyst. Moreover, in a previous study, they demonstrate that neutral Cu clusters after landing on the SiO support undergo structural rearrangement and exhibit rather cationic nature.[26]

Recently, we reported the structures of bare, cationic copper clusters Cu_n^+ (n = 3−10) obtained via IR spectroscopy in the 70−300 cm^{-1} spectral range.[27] Here, we present IR spectra to characterize the products formed upon reacting cationic Cu_n^+ clusters with hydrogen. IR spectroscopy employing IR free-electron lasers has proven to be a sensitive probe for the structure of metal clusters,[28] and clusters with hydrogen adsorbed.[29−32] To enable spectroscopy over the 350−1700 cm^{-1} spectral range, we utilize the intracavity free-electron laser FELICE.[33,34] We combine experimental IR multiple-photon dissociation (IRMPD) spectroscopy with density functional theory (DFT) calculations, including a systematic identification of candidate structures to be considered for assignment to the measured IR spectra by means of a global search algorithm.

METHODS

Experimental Section. Experiments were carried out in a molecular beam instrument equipped with a laser ablation source that is coupled to the free-electron laser for intracavity experiments.[33,34] Copper clusters were produced in a Smalley-type laser ablation source,[35] by vaporizing a 1 mm thick foil of isotopically enriched Cu-65 (STB Isotope GmbH), attached to a stainless steel rod that was simultaneously rotated and translated. For this, a pulsed Nd:YAG laser (532 nm) with the average pulse energy of 30 mJ was loosely focused on the Cu-foil. Clusters were formed through collisions with helium, injected into the source by a pulsed valve (General valve Series 9). After clusters were formed in a 6 mm diameter, 60 mm long growth channel, they were reacted with either pure H_2 or with D_2 diluted in helium (20%), injected by the second pulsed general valve into the reaction channel (6 mm diameter, 45 mm long). The mixture of helium, clusters, and cluster−molecule complexes then expanded into vacuum through a converging-diverging nozzle (∼0.9 mm diameter), forming a molecular beam. The beam then passed a 2 mm diameter skimmer, and was further shaped by a 2 mm high slit aperture, for better overlap with the IR laser beam. The molecular beam overlapped with the IR laser beam in the horizontal plane at a 35° angle in the extraction region of the orthogonal reflectron

time-of-flight (RTOF) mass spectrometer. After irradiation, all ions were extracted into the RTOF and detected on a microchannel plate detector. The experiment was operated at a 20 Hz repetition rate, whereas the FELICE laser operated at 10 Hz, allowing the registration of reference mass spectra, which are used to correct for fluctuations in the cluster production. The FELICE laser is an intracavity laser with high pulse energy, typically between 0.6 and 1 J, and a spectral bandwidth of approx. 0.5% full width at half-maximum (FWHM) of the central frequency. Because intracavity operation rules out the use of conventional attenuators to reduce the laser intensity, the whole molecular beam instrument is movable along the laser focus, allowing the use of different parts of the near-Gaussian laser beam and thereby tuning the laser fluence. For the current experiment, the instrument was positioned approx. 30 cm out of focus to prevent band saturation and increase the number of irradiated ions.

IRMPD spectra were recorded in the 350−1700 cm^{-1} frequency range. The spectra are presented as depletion spectra, where the depletion $D(\nu)$ at frequency ν is defined as

$$D(\nu) = \frac{I(\nu)}{I_0} \tag{1}$$

with $I(\nu)$ and I_0 the integrated intensity of the mass peak of the species of interest with and without IR irradiation, respectively. Depletion spectra are useful to assess whether a population of ions is made up of multiple isomers, but can suffer from ingrowth by the IR-induced fragmentation of, e.g., $[4Cu, 4H]^+$ resulting in the formation of $[4Cu, 2H]^+$. To mitigate such effects, we define the branching ratio $B(\nu)$ of Cu_n^+ clusters reacted with mH_2 molecules to all species containing Cu_n^+ clusters, given by

$$B(\nu) = \frac{\sum_{m=1,2,\cdots} I_{[nCu,2mH]^+}(\nu)}{\sum_{m=0,1,2,\cdots} I_{[nCu,2mH]^+}(\nu)} \tag{2}$$

and its equivalent B_0 with the laser off. We then define the IRMPD yield $Y(\nu)$

$$Y(\nu) = -\ln\left(\frac{B(\nu)}{B_0}\right) \tag{3}$$

At no point, any signal was observed in the $[nCu,mH]^+$ mass channel for *odd* m, indicative for loss of atomic H. This is in line with the significant energetic favorability of 2H-loss over H-loss as calculated with the computational setup described in the following section (see the Supporting Information for detailed results). The IRMPD yield spectra are corrected for the macropulse energy, inferred from coupling a small fraction of the IR light out of the cavity. The same light is used to calibrate the IR frequency by directing it onto a grating spectrometer.

Computational Section. To systematically find all of the possible local minima on the potential energy surfaces (PESs) an efficient global sampling algorithm is crucial since the number of local minima increases exponentially with system size. Therefore, we use the minima hopping (MH) method[36] as a highly efficient approach for PES exploration. This method has been used successfully in cluster structure prediction for both neutral and charged systems in several works.[37,38] We explore the energy landscape of $[nCu, 2H]^+$ (n = 4−7) clusters in an extensive study using DFT-based MH, which is implemented in the Atomic Simulation Environment

(ASE).[39] For all of the DFT calculations in this work, we employ the *ab initio* molecular simulation package (FHI-aims).[40] In our MH runs, we use the PBE exchange-correlation functional[41] with the default tight settings, which includes tier 1 and tier 2 basis functions for H and Cu, respectively. All calculations have been carried out including spin polarization, and we have verified that the electronic configuration with the smallest possible amount of unpaired electrons constitutes the electronic ground state of the local minima structures. For each cluster size, we run MH at least 10 times with different random starting structures, i.e., different points on the energy landscape, to scan the PES thoroughly. All of the local minima structures obtained from these MH runs for each size are carefully refined by environment descriptors[42] implemented in the FLAME code[43] to conveniently identify and remove potential duplicates. This way, we find all of the structures which have been reported before by Guvelioglu et al.[21] In addition, we also discover several new low-energy structures for each cluster size.

In the next step, we add basis functions from tier 3 for H and tier 2 for Cu and reoptimize all previously selected local minima using a force threshold of 10^{-4} eV/Å. Our convergence tests have shown that this larger basis set yields adsorption energies that are converged up to less than 5 meV (for a given functional). For the ensuing analysis, we consider the ≤ 15 structures with the lowest total energy for each cluster size, since additional local minima are (even) less likely to be formed under the experimental conditions relevant for this study. Reoptimizations of the selected local minima are also repeated with the PBE0[44,45] hybrid functional using the same computational settings. Finally, we calculate IR spectra for PBE and PBE0 for all of the reoptimized minima structures within the harmonic approximation for both the frequencies and the infrared intensities[46] using a finite difference approach (displacement step size, 0.01 Å) as implemented in the ASE package. Regarding the atomic mass of the copper atoms, we have verified that the two isotopes ^{63}Cu and ^{65}Cu yield negligible differences for the hydrogen-dominated spectral regime (*vide infra*) that is of interest for this work (see the Supporting Information).

We define the binding energy

$$E_{\text{b}}([n\text{Cu, 2H/2D}]^+)$$
$$= E([n\text{Cu, 2H/2D}]^+) - E(\text{Cu}_n^+) - E(\text{H}_2) \qquad (4)$$

as the difference between the total energy of the reaction product $E_{\text{b}}([n\text{Cu, 2H/2D}]^+)$ and the total energy of the global minimum structure of the cationic copper cluster $E(\text{Cu}_n^+)$ and the hydrogen molecule in its ground state $E(\text{H}_2)$. For Bader charge analyses, we employ the implementation by Tang et al.[47] To calculate energy barriers for H_2 dissociation, we calculate transition states with the climbing-image nudged elastic band (CI NEB)[48] technique. We employ its implementation in the ASE package using at least seven images between reactants and products to obtain converged minimum-energy paths provided in the Supporting Information. Throughout this work, both binding energies and energy barriers are zero-point energy (ZPE) corrected.

RESULTS AND DISCUSSION

Depletion Spectra. The depletion spectra for $[n\text{Cu, 2H}]^+$ are presented in Figure 1. Except for the spectrum for $[4\text{Cu, 2H}]^+$, all spectra show very large depletions: 0.2 for $[6\text{Cu},$
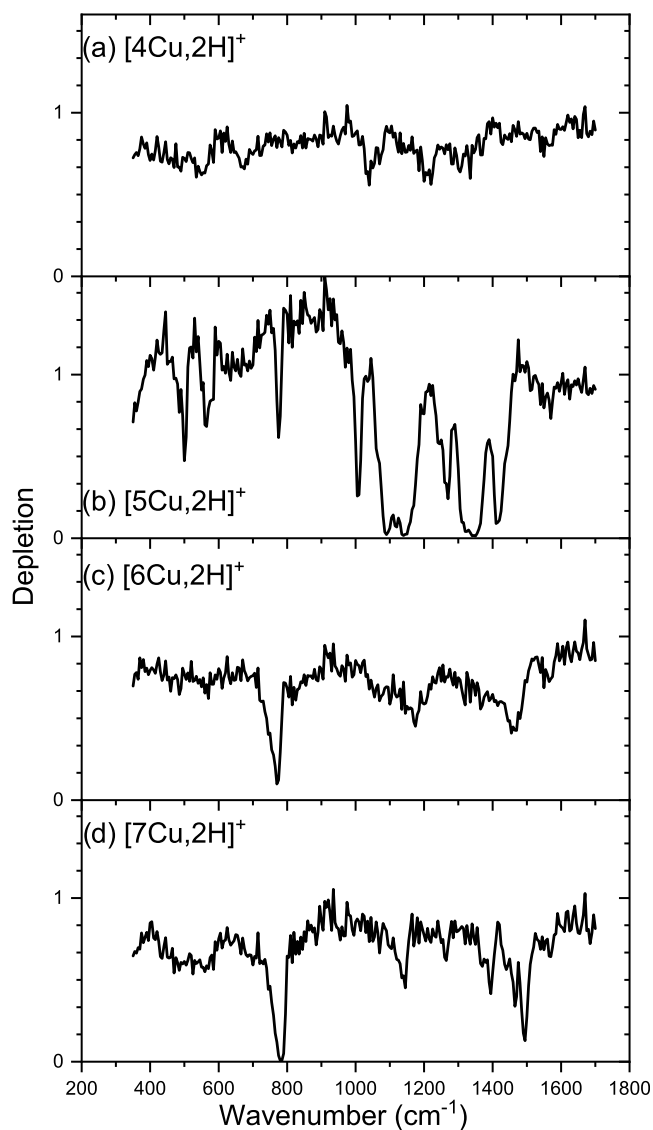

Figure 1. Depletion spectra of $[n\text{Cu, 2H}]^+$ for $n = 4-7$.

$2\text{H}]^+$, and approaching 0 for $[5\text{Cu, 2H}]^+$ and $[7\text{Cu, 2H}]^+$. Since the depletion indicates how much of the original population survives after the ions are exposed to IR radiation ($D = 1$ implies all population is left, $D = 0$ no population survives), the spectra for $[5\text{Cu, 2H}]^+$, $[6\text{Cu, 2H}]^+$ and $[7\text{Cu, 2H}]^+$ all appear originating from one dominant isomer, or by multiple isomers sharing one major band. In contrast, the depletion for $[4\text{Cu, 2H}]^+$ never goes below 0.6, suggesting that this spectrum is made up of multiple isomers, with none strongly dominant. Especially the spectrum for $[5\text{Cu, 2H}]^+$ appears to indicate one dominant isomer, which will facilitate the assignment. The gain in the region around 800 cm^{-1} ($D > 1$) in the spectrum of $[5\text{Cu, 2H}]^+$ originates from the fragmentation of $[5\text{Cu, 4H}]^+$, as can be seen from the mass spectrum in Figure S1. This ingrowth will be corrected for by presenting the spectra as depletion yield spectra, as outlined in eq 3. We will first discuss the spectra of $[5\text{Cu, 2H}]^+$ and $[5\text{Cu, 2D}]^+$ to investigate which level of theory, and which scaling factor are most adequate for assignment, before discussing other species.

Cu$_5^+$. The spectrum of $[5\text{Cu, 2H}]^+$, depicted in the top left panel of Figure 2, shows the best signal-to-noise ratio and the
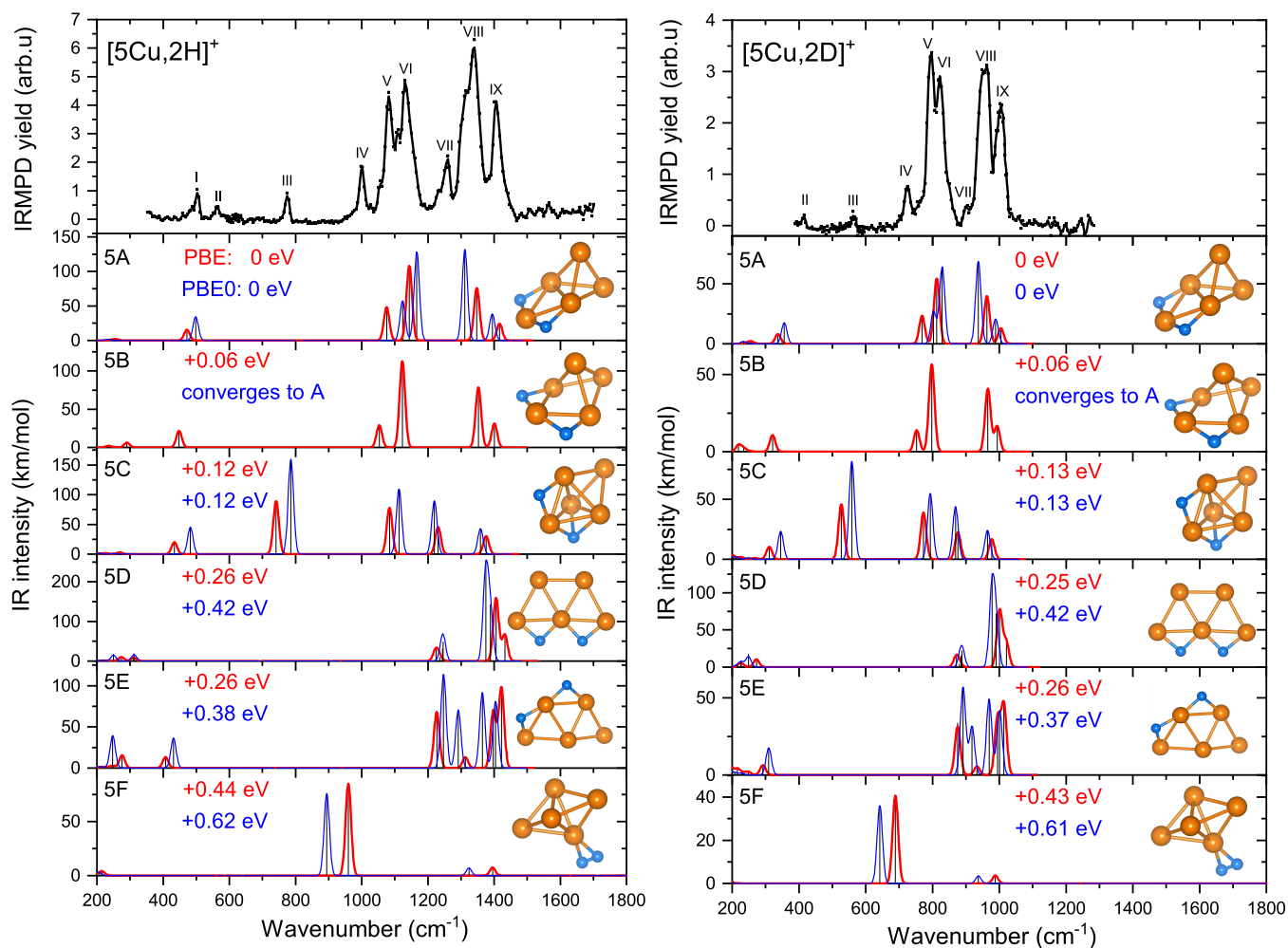
Figure 2. Experimental IRMPD spectra of $[5Cu, 2H]^+$ (top left) and $[5Cu, 2D]^+$ (top right), accompanied by a five-point adjacent average (black line). The experimental spectra are compared to calculated harmonic spectra of various isomers obtained with the PBE (red sticks/curves) and PBE0 (blue) exchange-correlation functionals. Harmonic frequencies were scaled with a factor of 0.98 and intensities convoluted with a 20 cm^{-1} FWHM Gaussian line shape function. The ZPE-corrected relative energy of each isomer (structure shown in each panel) with respect to the global minimum (structures 5A in each column) is indicated as well.

narrowest bandwidth ($\sim$20 cm^{-1}) among all measured spectra. The spectrum exhibits nine clear bands that are indicated by Roman numerals. The band frequencies are listed in Table 1, along with the observed bands for $[5Cu, 2D]^+$, their assignments to structures, which we discuss below, and the ratio of the frequencies of observed and calculated bands for $[5Cu, 2H]^+$ and $[5Cu, 2D]^+$, respectively.

Most of the bands observed for $[5Cu, 2H]^+$ are isolated and well resolved, except for bands V and VI, that overlap at the base. Bands VII, VIII, and IX are better resolved, but VII and VIII have shoulders on the low-frequency side, suggesting the presence of even more overlapping bands. The spectrum for the $[5Cu, 2D]^+$ system (top right panel in Figure 2) has a quite similar shape, albeit with a slightly larger average bandwidth of 33 cm^{-1}, and of course a significant redshift caused by the doubling of the reactant's molecular mass. Similar to the spectrum of $[5Cu, 2H]^+$, bands V and VI are overlapping, as are now bands VII, VIII, and IX. The similar shapes of the spectra suggest that the modes observed all involve significant motion of the hydrogen, molecular or dissociative form. By analyzing the experimental band positions, we can relate the bands in the spectrum for $[5Cu, 2H]^+$ and $[5Cu, 2D]^+$ to each other, and thus allow for a more stringent set of observables

used for assignment. As a consequence, we label the bands observed in the $[5Cu, 2D]^+$ spectrum according to their counterparts in the spectrum for $[5Cu, 2H]^+$. The found correlation for the spectra is such that the frequencies of the observed bands are reduced by a factor of 1.35−1.40 upon reaction with D_2. That this ratio is close to the textbook value of $\sqrt{2}$ expected for H−D substitution is an additional strong indication that all bands in this spectral region are dominated by motion of the H atoms. The ratios for each individual band are included in Table 1.

Our calculations provide the final proof for the domination of the measured spectra by H atom motion: Figure 3a shows the H- and Cu-projected IR spectra for the lowest-energy $[5Cu, 2H]^+$ structure (5A in Figure 2), which are obtained by weighing each mode with the fraction of hydrogen and copper atom motions described by the corresponding displacement vector in mass-weighted coordinates. Modes with frequencies larger than 400 cm^{-1} show only a negligible contribution of the Cu atoms. This trend is the same for all other structures $[nCu, 2H]^+$, $n = 4-7$, as evidenced by additional plots equivalent to Figure 3a. Furthermore, we have calculated the overlaps of the aforementioned normal mode displacement vectors for all $[nCu, 2H]^+$ and corresponding $[nCu, 2D]^+$ local minima

Table 1. Observed Vibrational Bands ν_{H_2} and ν_{D_2} for $[nCu, 2H]^+$ and $[nCu, 2D]^+$ with $n = 4-7$, Respectively, Their Assignments, and the Corresponding Frequencies from the Calculations with the PBE Functional (Including Scaling with a Factor 0.982)^a

band	structure assigned	$[nCu, 2H]^+$ ν_{H_2} (in cm^{-1}) obs.	calc.	$[nCu, 2D]^+$ ν_{D_2} (in cm^{-1}) obs.	calc.	ratio ν_{H_2}/ν_{D_2} obs.	calc.
				$n = 4$			
I	F	485	450		318		1.42
II		551					
III	C	670	837	510	600	1.31	1.41/1.34
IV	E/F	1030	1054/1057	780	746	1.32	1.41
V	D	1200	1236	924	880	1.30	1.40
VI	A/B	1290	1387/1350	977	992/961	1.32	1.40/1.40
VII	F	1555	1448		1028		1.41
				$n = 5$			
I	A/B/C	503	471/448/433		334/321/312		1.41/1.40/1.39
II		566		416		1.36	
III	C	775	742	562	525	1.38	1.41
IV	F	1002	959	726	689	1.38	1.39
V	A/B/C	1081	1074/1053/1086	798	767/751/772	1.35	1.40/1.40/141
VI	A/B	1135	1145/1121	822	813/797	1.38	1.41/1.41
VII	C	1260	1228	905	875	1.39	1.40
VIII	A/B	1330	1348/1352	957	963/966	1.39	1.40/1.40
IX	A/B/C	1406	1416/1400/1375	1003	1005/993/977	1.40	1.41/1.41/1.41
				$n = 6$			
I	G	770	920	576	662	1.34	1.39
Ia	A	830	824	620	584	1.34	1.41
II	A	1067	1083	798	771	1.34	1.40
III	A	1166	1186	866	843	1.35	1.41
IV	C	1306	1262				
V	A	1392	1393	982	991	1.42	1.41
VI		1453		1090		1.33	
				$n = 7$			
I	D	784	904	583	646	1.34	1.40
II	A	1135	1185				
III		1255					
IV	A	1386	1381				
V	F	1488	1417	1125	1009	1.32	1.40

^{a}The last column lists the ratios ν_{H_2}/ν_{D_2} for bands that have been identified to correspond to one another as described in the text.

structures ($n = 4-7$). Figure 3b compiles the results for structure 5A, which—together with Figure 3a—confirm the hydrogen−deuterium correlation of the bands. Again, results for all other structures and cluster sizes are compiled in the Supporting Information and follow the trend showcased here.

To assign these experimental spectra to geometrical structures, we compare them to calculated spectra of energetically favorable candidate structures found via the global sampling. In Figure 2, the scaled vibrational spectra of the most plausible candidates are compared to the experimental spectra, the full list can be found in the Supporting Information. The lowest-energy structures found are three-dimensional structures with dissociated H$_2$ with 5A shaped as a tetrahedron capped by a bridging Cu, and the others reminiscent of the Cu$_5^+$ trigonal bipyramid cluster structure.[27] Two-dimensional structures containing a W-shaped cluster and only differing in the position of the bridge adsorption site of the hydrogens are found isoenergetic at 0.26 eV for PBE, whereas PBE0 calculated them at 0.42 (structure 5D) and 0.38 eV (5E), respectively. Only at 0.44 eV (PBE0

0.62 eV), the first structure with molecularly bound hydrogen, structure 5F, is found.

The lowest-energy structure 5A calculated for the [5Cu, 2H]$^+$ shows good agreement with the experimental spectrum for both functionals. Bands I, V, VI, VIII, and IX can readily be explained PBE-predicted bands at 480, 1094, 1166, 1373, and 1442 cm^{-1}, respectively. The agreement with PBE0 is only slightly poorer, most clearly demonstrated by a smaller frequency spacing between the two strongest bands predicted at 1229 and 1382 cm^{-1}, than what is observed between bands VI and VIII. On the other hand, the mode that can likely be assigned to experimental band I appears better predicted by PBE0 at 525 cm^{-1}. Structure 5B is also a potentially good candidate to explain bands I, V, VI, VIII, and IX, since it exhibits a spectrum very similar to that of structure 5A and is only 0.06 eV higher in energy for PBE. In comparison to the spectrum for 5A, the bands are slightly shifted, which, if the assignment holds, could explain the broadening of the experimental bands. In particular, band I has an asymmetric shape that could readily be explained by bands predicted at 456 cm^{-1} for 5B and at 480 cm^{-1} for 5A. Employing PBE0,
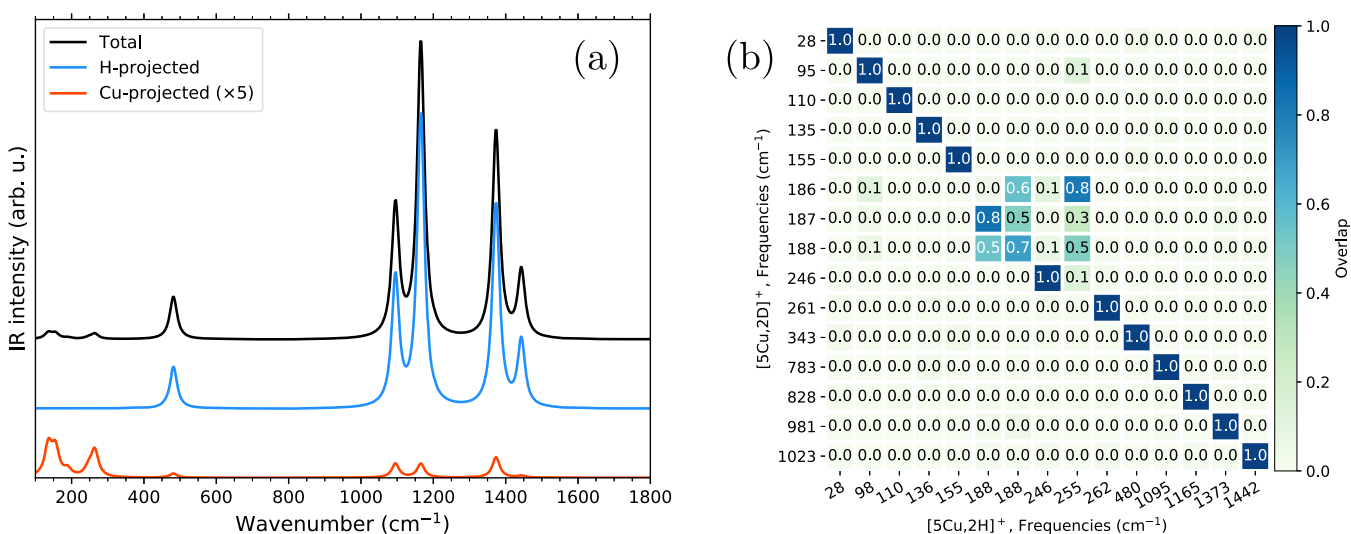
Figure 3. (a) H- and Cu-projected IR spectra for the lowest-energy [5Cu, 2H]$^+$ structure (5A in Figure 2). (b) For the same structure, overlap of [5Cu, 2H]$^+$ and [5Cu, 2D]$^+$ normal mode displacement vectors (in mass-weighted coordinates) belonging to the corresponding 15 (= 3 × 7−6) nonzero frequencies indicated on the *x*- and *y*-axes, respectively. Both plots are based on the PBE functional, and the frequencies have not been scaled.

structure 5B collapses into 5A during optimization. The similarity is confirmed when taking into account the spectrum for the deuterated species: bands V, VI, VIII, and IX for [5Cu, 2D]$^+$ appear safely assigned to PBE-predicted bands at 783, 828, 981, and 1023 cm^{-1}, respectively. Here too, PBE0 is outperformed by PBE due to the spacing between bands VI and VIII.

Because the spectrum of structure 5A can explain the four most intense experimental bands for both [5Cu, 2H]$^+$ and [5Cu, 2D]$^+$, the bands assigned above are used to derive a scaling factor, needed to correct for anharmonic effects not taken into account in the frequency calculations, but also for slight red-shifting that is common to IRMPD.[49] A scaling factor is obtained by fitting experimental bands V, VI, VIII, and IX from the [5Cu, 2H]$^+$ spectrum and their counterparts from the [5Cu, 2D]$^+$ spectrum to the assigned theoretical frequencies. The scaling factors found for PBE are 0.982 and 0.949 for PBE0. For these fits, the coefficient of determination (R^2) is 0.996, significantly higher for PBE than for PBE0 (0.985). Simultaneously, the 95% confidence limit of the scaling factor is twice smaller for PBE (0.01) than for PBE0 (0.02).

Once the scaling factors are established, all other calculated spectra are also scaled with these values, and we attempt to assign the remaining bands: II, III, IV, and VII.

Band III seems most straightforward: the only structure showing any activity in the 700−800 cm^{-1} spectral range is structure 5C, and this structure also provides a plausible explanation for band VII. The two remaining strong bands predicted for 5C are likely submerged under bands already assigned to 5A. PBE does not perform particularly better than PBE0 for these two bands. This assignment is consistent with that for the deuterated analogue: bands III and VII are plausibly explained by 5C with other bands coinciding with bands for structure 5A.

That leaves bands II and IV, where we will neglect the first because (a) we do not see a trivial assignment and (b) it is fairly weak. Band IV, however, appears reasonably matched with the strongest band at 959 cm^{-1} of structure 5F, the

lowest-energy structure with molecularly adsorbed H$_2$. Strikingly, the frequencies predicted by PBE and PBE0 differ from each other by about 100 cm^{-1}, with PBE closest, but already off by an uncomfortably large 40 cm^{-1}. The remaining low-energy structures 5D and 5E only show bands above 1200 cm^{-1} in both calculations, but these bands are right in the region where 5A and 5B have their strongest bands. If 5D and 5E are there, they are likely not in large abundance. Given the shape of the copper cluster, it appears reasonable to suspect that their formation from the bare Cu$_5^+$ structure, a trigonal bipyramid,[27] requires crossing a relatively high-energy barrier.

Thus, all experimental bands except band II could be assigned to isomers A, B, C, and F, since they have absorption lines at similar frequencies. The spectrum is dominated by structures A and B, with small contributions of C and F. Structures D and E cannot be fully excluded, but if present, their contributions would be small. All of these conclusions can be verified by the comparison with the deuterated system [5Cu, 2D]$^+$. Except for band I, which has shifted out of the spectral window probed here, all bands for [5Cu, 2D]$^+$ can be assigned to the same bands as for [5Cu, 2H]$^+$, which have merely shifted down in frequency. The calculated spectra are all highly similar to those calculated for [5Cu, 2H]$^+$, except, of course for the systematic redshift.

This assignment appears in conflict with the conclusion drawn from the depletion spectrum, that the spectrum is dominated by one isomer, or at least has all isomers share the strong bands between 1000 and 1400 cm^{-1}. Especially band IV, assigned to structure 5F, has no such bands in other assigned structures, and is therefore flagrantly at odds with the conclusion drawn from the depletion spectrum. We speculate that the Cu$_5^+$ cluster could be highly fluxional, something which was earlier invoked as a potential factor that could enhance catalytic activity.[50] If this were the case, one could envision that the IR spectrum of the fluxional system consists of a sum of the individual spectra. Given the difference between the structure of the bare cluster, a trigonal bipyramid,[27] mirrored in isomer 5F, and the cluster structure in isomer 5A, the fluctionality should be able to overcome a
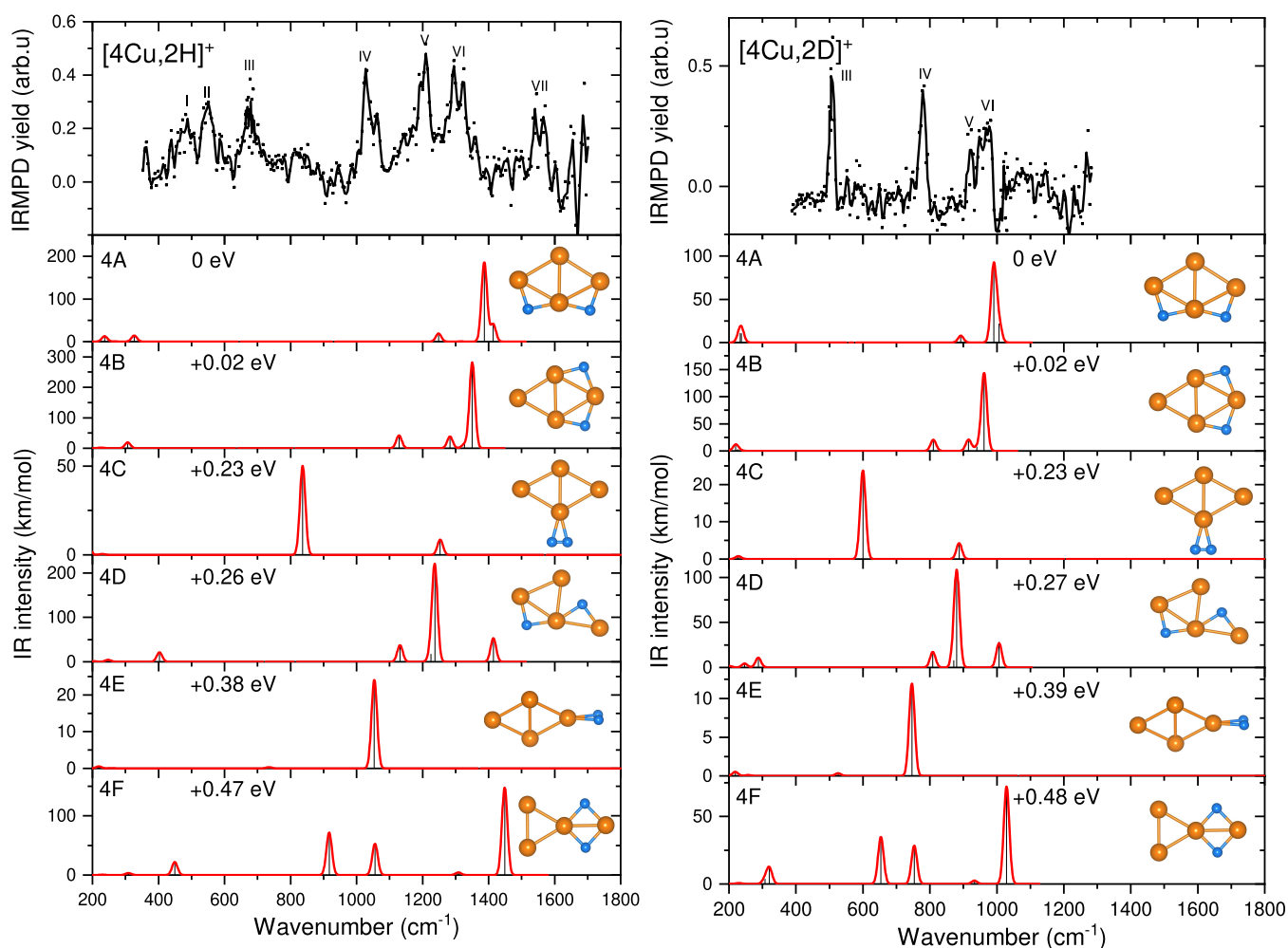
Figure 4. Same as Figure 2, but for $[4Cu, 2H]^+$ (left column) and $[4Cu, 2D]^+$ (right column). Calculated spectra are shown for the PBE functional only (red line).

relatively large structural reorganization. The outcome of an investigation into this merits a publication by itself.[51,52]

Here, we conclude that all assigned structures have hydrogen dissociatively bound to the copper cluster, except for isomer 5F, and that the spectra are more accurately predicted by the PBE functional, in combination with a scaling factor of 0.982. First, because the fit for the scale factor described above has a higher confidence value, and second, because a scaling factor closer to unity is found. As a consequence, we will in the remainder only employ this combination to identify the structures for other cluster sizes.

Cu$_4^+$. As could be expected from the relatively low depletions observed for $[4Cu, 2H]^+$, the IRMPD yield spectrum, shown in the top left panel of Figure 4, is rather lower in signal-to-noise ratio than that for $[5Cu, 2H]^+$, making the assignment also more complex. The spectrum exhibits seven bands, all labeled with Roman numerals. The clearest bands are found at 670, 1030, 1200, and 1295 cm^{-1}. The broadening at the base suggests that they could consist of multiple overlapping bands.

The spectrum of the deuterated complex (Figure 4, top right) is of similar quality and only has four bands at 510, 780, 924, and 977 cm^{-1}, respectively. Just as before for $[5Cu, 2H/2D]^+$, we have verified that all modes in this region involve the motion of a hydrogen or deuterium atom, the bands for $[4Cu,$

$2H]^+$ and $[4Cu, 2D]^+$ can be safely correlated through their frequency shifts, and the bands observed for $[4Cu, 2D]^+$ are labeled accordingly. We do note that the ratios of frequencies observed for $[4Cu, 2D]^+$ to those for $[4Cu, 2H]^+$ are 1.30–1.32, and thus slightly smaller than the ratios found for $[5Cu, 2D]^+$ and $[4Cu, 2H]^+$, suggesting a larger involvement of Cu motion in the vibrations.

From the depletion spectrum in Figure 1, it was already suggested that the $[4Cu, 2H]^+$ spectrum is the result from a mixture of several isomers. When comparing the experimental spectrum to the selection of the theoretical spectra (additional structures are provided in the Supporting Information), it becomes clear that none of them can explain all bands on its own, strengthening the multi-isomer hypothesis.

When comparing the experimental spectrum to calculated spectra of low-energy isomers of $[4Cu, 2H]^+$, one cannot fail to note the relative simplicity of the calculated spectra: all of them are dominated by a single band, sometimes accompanied by bands with intensities lower by at least a factor of 5. The exception to this is formed by 4F, the only isomer *not* based on the rhombus geometry of bare Cu$_4^+$.[27] Rather, it is a 2D structure based on an equilateral triangle, with the last Cu on top of one of the vertices. Structures 4A and 4B are relatively similar in energy, formed by the Cu$_4^+$ rhombus with H atoms adsorbed in-plane on bridge sites.
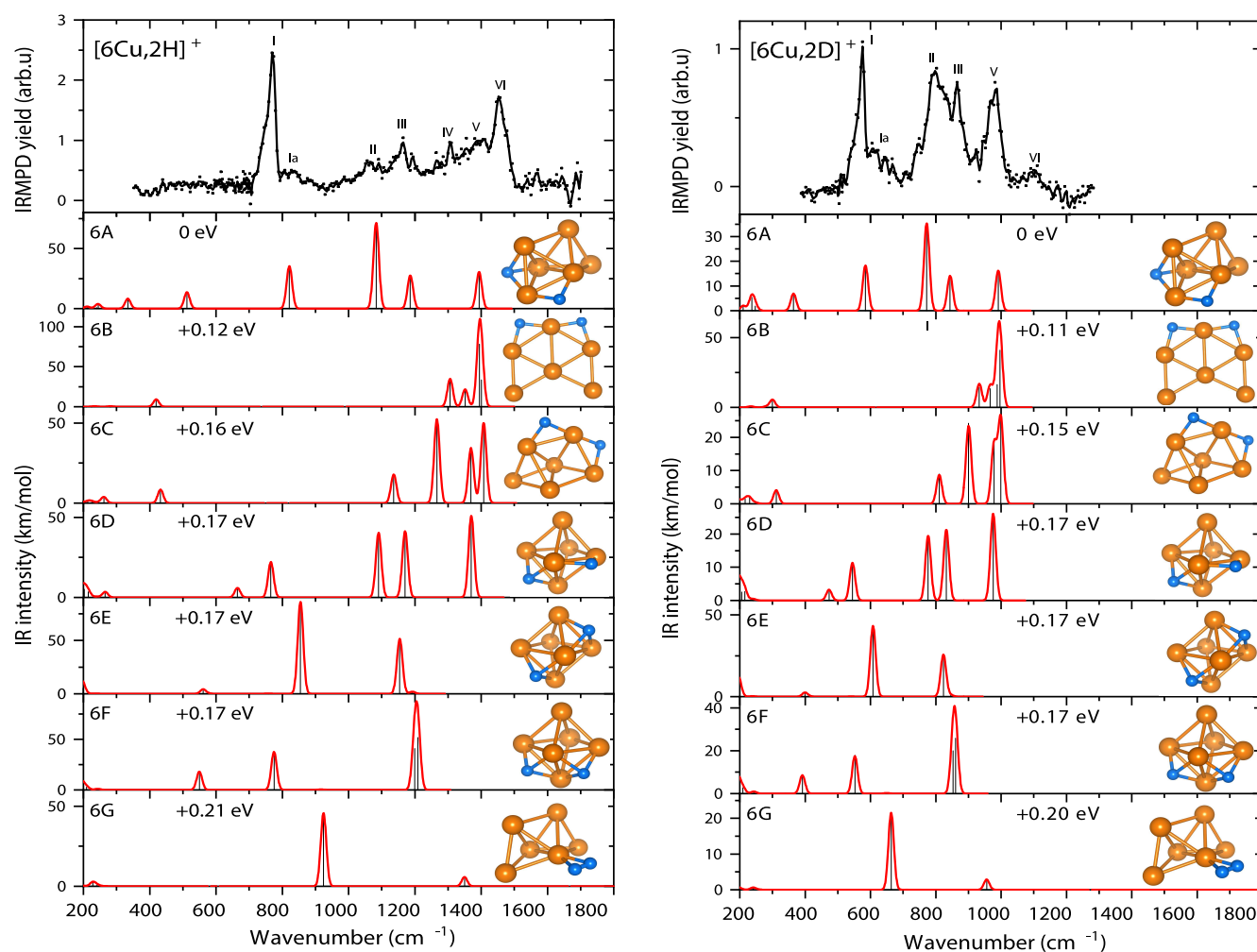
Figure 5. Same as Figure 2, but for $[6Cu, 2H]^+$ (left column) and $[6Cu, 2D]^+$ (right column). Calculated spectra are shown for the PBE functional only (red line).

Given the simplicity of the calculated spectra and the complexity of the observed spectrum, it is not easy to assign bands identified in the latter. We start with band IV, which for both the $[4Cu, 2H]^+$ and $[4Cu, 2D]^+$ systems appears relatively safe to assign to structure 4E, with molecular hydrogen adsorbed intact to the sharp apex of the rhombus. The vibration involved is the concerted antisymmetric Cu-H stretch. Band V can be explained by bands from structure 4D, which has other bands at 402, 1132, and 1414 cm^{-1}. These lower-intensity bands can be hidden in the noise or below stronger bands. Assignment of band VI at 1295 cm^{-1} is not so straightforward. Structures 4A and 4B both offer bands at 1387 and 1350 cm^{-1}, respectively, which appear quite off. For the deuterated species, band VI at 977 is matched better by them, now found at 992 and 961 cm^{-1}. Given this match, we assign band VI to the near-isoenergetic lowest-energy structures.

Of the bands found in both experimental spectra, we are now left with band III. While none of the predicted structures has modes close in frequency for this band, we are tempted to assign this to structure 4C, where the most intense band is due to the intermolecular stretch vibration between the copper cluster and the hydrogen molecule. This mode is predicted 150 cm^{-1} higher than the experimental value, making the assignment rather shaky. However, similar mismatches for this mode have been found by Swart et al.[29] for H$_2$ adsorbed to

cationic Ni clusters. Likewise, a comparably large overestimation of the H−H stretch mode by DFT calculations has been reported for H$_2$ bound to Cu$^+$ ions in zeolites.[53] This assignment is not inconsistent when comparing with $[4Cu, 2D]^+$, for which the predicted frequency is off by 90 cm^{-1}. As also evidenced by a very recent benchmark study, an accurate description of H$_2$-transition-metal bonding can still pose a challenge for DFT.[54]

Further bands were found for $[4Cu, 2H]^+$ only. Band VII is attributed to structure 4F, with its other bands at 450, 917, and 1057 cm^{-1} potentially responsible for band II, the bump between 800 and 900 cm^{-1}, and additional intensity for band IV, respectively. Band I could potentially be assigned to structure 4D.

Cu$_6$$^+$. The spectrum of $[6Cu, 2H]^+$, shown in Figure 5, is dominated by a strong band at 770 cm^{-1} and further contains a broad absorption band, which starts at 1000 cm^{-1}, and gradually grows before it abruptly ends just below 1500 cm^{-1}. Several local maxima in this band are identified and labeled. The spectrum for the deuterated species is more compact and better resolved, showing four main bands, which, based on their frequency correlation with bands for $[6Cu, 2H]^+$, are labeled with the appropriate numerals. As will become clear from the discussion below, we have also chosen to label a high-
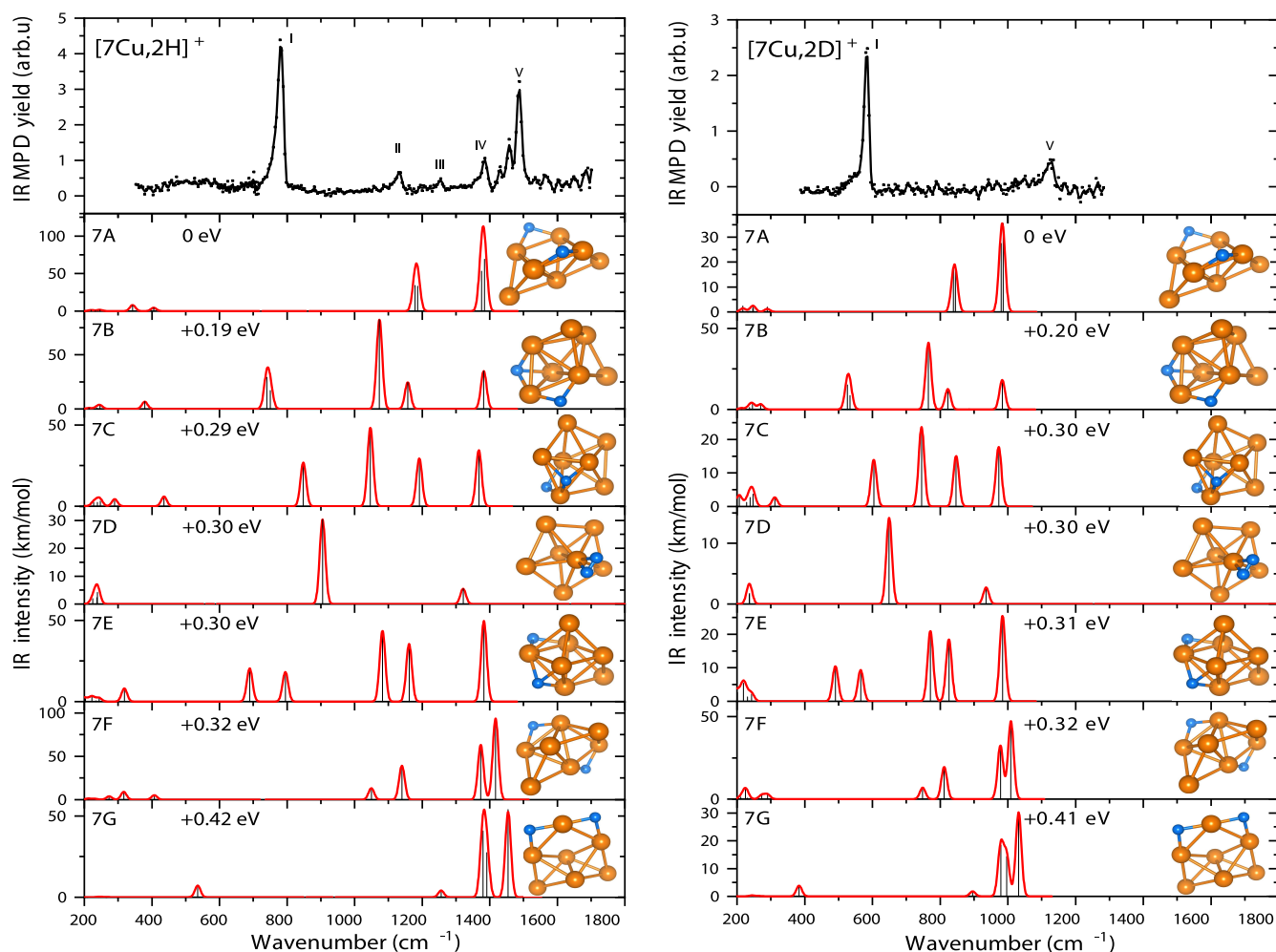
Figure 6. Same as Figure 2, but for $[7Cu, 2H]^+$ (left column) and $[7Cu, 2D]^+$ (right column). Calculated spectra are shown for the PBE functional only (red line).

frequency shoulder of band I in both spectra and a low, bumpy feature around 1100 cm^{-1} in the spectrum of $[6Cu, 2D]^+$.

The assignment of the spectra for $[6Cu, 2H]^+$ and $[6Cu, 2D]^+$ is again far from straightforward. The calculations yield a large number of isomers that are within 0.3 eV from the putative global minimum, and even within 0.02 eV four competing structures are found. A selection of these is shown in the lower panels in Figure 5; the 15 lowest-energy structures are shown in the Supporting Information. What is most striking about these spectra is the observation that most of them are dominated by bands in the 1000−1500 cm^{-1} spectral range. If bands in the vicinity of band I (770 cm^{-1}) are found, they are accompanied by stronger bands at higher frequencies, making it difficult to assign band I to any of these structures. This is, for instance, the case for structures 6A (although its band at 824 cm^{-1} appears a bit too high in frequency to even consider it), 6D, and 6F.

The only structures for which an intense band at lower frequencies is accompanied by weaker bands at higher frequencies are structures 6E and 6G. Energetically, these structures are quite close, and for neither the 770 cm^{-1} band is predicted particularly well. Given the ratio between the 855 and the 1154 cm^{-1} bands for 6E, we tend to favor structure 6G, with a band at 920 cm^{-1}, and a much weaker second band at 1350 cm^{-1}. Band I at 770 cm^{-1} is thus assigned to a mode

that is predicted to lie more than 150 cm^{-1} higher in frequency, making it quite unappealing, were it not for the nature of this mode: structure 6G's 920 cm^{-1} band is the intermolecular stretch vibration of molecular H_2 on the cluster surface, the same mode offering the only plausible explanation for band III for $[4Cu, 2H]^+$.

Having assigned band I on these grounds does not make the assignment of the remaining bands much easier. One would be tempted to compare the spectrum for $[6Cu, 2D]^+$ to the lowest-energy isomer 6A, and directly assign all bands (including the bump labeled II) to the four bands predicted between 400 and 1000 cm^{-1}. Unfortunately, this assignment does not hold when examining the same comparison for $[6Cu, 2H]^+$. Although bands Ia to V could plausibly be explained by 6A (the predicted intensity for band II being the main dissonant), they certainly cannot account for band VI or the continuous absorption between bands III and V. For bands IV and V, the continuous absorption one could invoke the presence of, for instance, isomer 6B or 6C, with only 0.12 and 0.16 eV from the putative global minimum. Both are consistent with the spectrum for $[6Cu, 2D]^+$. That leaves band VI. The rather surprising intensity drop this band incurs in the spectrum for $[6Cu, 2D]^+$ makes one suspicious band VI in the $[6Cu, 2H]^+$ spectrum should not have its counterpart in band V in the $[6Cu, 2D]^+$ spectrum; however, the frequency

ratio for the latter combination is 1.28, whereas all other bands have ratios in the range of 1.34−1.35. The frequency ratio for bands VI is with 1.33 much closer to the other ratios found. We can thus only speculate that one of the stronger bands in the predicted spectra for isomers calculated for $[6Cu, 2H]^+$ is underestimated by the current level of theory. We hope to resolve this in the future employing *ab initio* molecular dynamics calculations. Although the assignment is thus not 100% proof, we can conclude that adsorption of H_2 onto Cu_6^+ leads to a mixture of molecularly and dissociatively bound structures.

Cu_7^+. The final system we discuss is that of Cu_7^+ reacted with hydrogen. Spectra for $[7Cu, 2H]^+$ and $[7Cu, 2D]^+$ are displayed in Figure 6. The spectrum for $[7Cu, 2H]^+$ is dominated by two bands: band I at 784 cm^{-1} and band V at 1488 cm^{-1}. Three minor bands are found between 1000 and 1400 cm^{-1}, and it could be argued that band V is accompanied by minor side bands. In the spectrum for $[7Cu, 2D]^+$, only bands I and V are identified, at frequency ratios of 1.32 and 1.34, similar to the values found for Cu_6^+.

Assignment of band I is again not easy. Structure 7B has a band close, but its intensity relative to the other bands predicted for 7B is such that it is not easy to assign it. Similar arguments hold for 7C and 7E. The lowest-energy isomer with molecular H_2, 7D at 0.30 eV from the lowest-energy structure is off by more than 100 cm^{-1}, but it is the only isomer dominated by one intense band at lower frequencies. In analogy to the Cu_4^+ and Cu_6^+ cases, we assign band I to this structure.

The further assignment is even more ambiguous. Bands II and IV could potentially be assigned to structure 7A, but they are not found for $[7Cu, 2D]^+$, so it is difficult to confirm this. For band V, however, no plausible assignment can be found based on the currently found structures. For lack of any other arguments, we currently assign it to 7F, which has a doublet of bands predicted at too low frequencies, but its doublet structure is reminiscent for the observed side bands for band V. If this assignment were to be assumed correct, the applied scaling factor of 0.982 should rather be 1.03. A positive scaling factor is not unheard of,[55] but it is not a very satisfactory assignment. We deem an alternative assignment to structure 7G more unlikely given the ratio of intensities predicted for its two bands. Although we cannot completely rule out to have missed a relevant structure for $[7Cu, 2H/2D]^+$, we consider our global sampling for this like for all other cluster sizes to be rather extensive—given the fact that we have automatically found all of the minima structures that Cheng and co-workers have constructed manually for H_2 adsorption on neutral Cu_7 clusters.[20,21] Instead, future work needs to show whether the exchange-correlation functional or the harmonic approximation is to be blamed for the dissatisfactory agreement with the experimental data.

Discussion. The discussion of the experimental and calculated structures for $[nCu, 2H]^+$ and $[nCu, 2D]^+$ shows that even for these relatively small systems, it can be rather complicated to determine the structure. Although the assignment for $[5Cu, 2H]^+$ and $[5Cu, 2D]^+$ to structures with dissociatively bound H_2 appears relatively straightforward, all other spectra required assuming an isomeric mixture. Even then, the calculated spectra did not allow for completely convincing assignment in all cases.

In spite of this uncertainty, the current assignments of the IR spectra for $[nCu, 2H/2D]^+$ do indicate that the binding of H_2

appears very sensitive to the size of the cluster. This raises the question why hydrogen prefers one cluster size to the other. To answer this question, the binding energies for all structures found in the structure search are displayed in Figure 7.
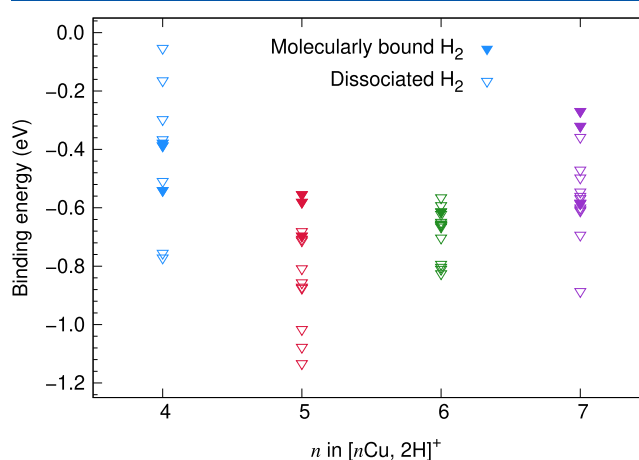

Figure 7. Distribution of binding energies calculated with the PBE functional for $[nCu, 2H]^+$, $n = 4-7$ (blue, red, green, and purple symbols, respectively). For each cluster size, isomers with molecularly bound (dissociated) H_2 are indicated by filled (empty) symbols.

Although one should be careful interpreting such a distribution, it appears that there is an overall stronger binding of H_2 to Cu_5^+ than to Cu_4^+, Cu_6^+, and Cu_7^+. In their DFT study of hydrogen chemisorption on neutral copper clusters, Cheng and co-workers have identified Cu_4 to bind dissociated H_2 most strongly and argued that the sharp-corner copper atom allows stronger overlap with their $4s$ orbital.[20,21] The absolute binding energies cannot be compared due to the fact that we study cationic clusters with a different (more accurate) computational setup including a systematic structure search, but the trend is certainly similar.

Although the dissociative adsorption of H_2 may thus be thermodynamically more favorable to Cu_5^+ than to the other cluster sizes investigated, there could also be kinetic arguments why dissociative binding to Cu_5^+ is more dominant. To understand this better, we have performed transition-state calculations for the cluster with the weakest bonds, Cu_4^+, and with the strongest, Cu_5^+. The reaction paths linking the lowest-energy structures for molecular and dissociated H_2 are illustrated in Figure 8.

For the rhombic Cu_4^+, adsorption of H_2 leads to the formation of the entrance complexes 4E (with H_2 bound to the acute apex) or 4C (with H_2 bound to the obtuse apex), with binding energies of −0.54 and −0.39 eV, respectively. This sizable difference in binding energies can be rationalized by comparing the Bader charges for these two complexes. In the case of 4C, H_2 donates about 0.3 electrons of its σ-bond to Cu_4^+, whereas it is only about 0.1 in 4E. The orbital overlap is thus less pronounced when the molecule and the cluster are not in the same plane. To form the global minimum 4A from 4C, H_2 is cleaved followed by H-transfer over the obtuse apex, passing the transition state TS4.2 at +0.15 eV with respect to the reactants. 4B can be formed either from 4A by deforming the rhombus, passing TS4.3 at −0.54 eV, or from 4E, where H cleavage is effectuated by a temporary deformation of the rhombus into a tetrahedron; the latter requires passing from TS4.1 at +0.22 eV. The lowest-energy barrier that needs to be
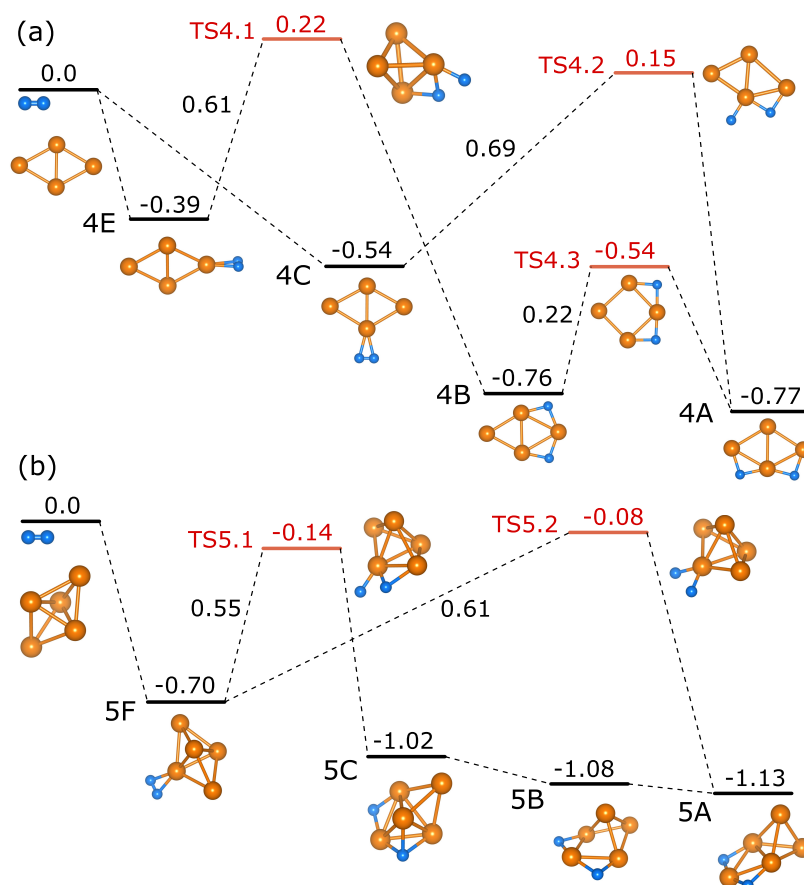
Figure 8. Calculated minimum-energy paths for H_2 dissociation over (a) Cu_4^+ and (b) Cu_5^+ based on the PBE functional. The hydrogen binding energies (see eq 4) for each local minimum structure (black) and the concomitant barrier heights due to the calculated transition states (red) are given in eV. All paths start from infinite separation of the hydrogen molecule and the cluster to mimic H_2 in the gas phase with $E_b = 0$.

overcome for H_2 cleavage is thus endothermic, but only by 0.15 eV, an energy that is probably available under room temperature conditions at which the experiment takes place. Collisions with the helium carrier gas are likely helping to stabilize the entrance complexes but not sufficiently frequent to prevent all complexes from dissociation.

Adsorption of H_2 onto trigonal bipyramidic Cu_5^+ leads to the much stronger bound entrance complex 5F (−0.70 eV). In contrast to Cu_4^+, Cu_5^+ offers an exothermic barrier TS5.1 for H_2 cleavage at −0.14 eV, linking 5F to 5C with two H atoms adsorbed in hollow positions. The formation of 5B and subsequently 5A from 5C is essentially barrierless. In an alternative pathway, 5A can also directly be formed from the entrance complex 5F over the only barely exothermic TS5.2 at −0.08 eV. Thus, once the entrance complex is formed, the energy available is sufficient to overcome the H_2 cleavage barrier. The larger binding energy of H_2 to Cu_5^+ thus effectively reduces the barrier for H_2 cleavage, providing a satisfactory explanation why the spectrum for $[5Cu, 2H]^+$ is dominated by structures with dissociatively bound H_2. Interestingly, the barrierless conversion between the near-isoenergetic species 5C, 5B, and 5A suggests that they may coexist in a dynamic equilibrium. Such a "fluxional" behavior could be evidenced by calculating the IR spectrum via ab initio molecular dynamics studies, which we are currently undertaking.

CONCLUSIONS

We have recorded the IRMPD spectra of the products formed upon reacting cationic Cu_n^+ clusters ($n = 4−7$) with hydrogen. The spectra are interpreted using DFT calculated IR spectra for several potential reaction products, obtained using a minima hopping search procedure. The spectra all are assigned to a mixture of at least two structural isomers, with dominant contributions from structures with molecularly adsorbed H_2 for $n = 4, 6, 7$. In contrast, the spectrum for the $[5Cu, 2H]^+$ product formed upon reacting Cu_5^+ is dominated by dissociatively bound hydrogen. The observed hydrogen cleavage is rationalized by calculations of the reaction paths for Cu_5^+, where barriers toward H_2 cleavage are found to be at energies below that of the reactants, effectively enabling the reaction.

ASSOCIATED CONTENT

ⓢ Supporting Information

The Supporting Information is available free of charge at https://pubs.acs.org/doi/10.1021/acs.jpca.0c11527.

Local minima structures based on PBE (ZIP)
Mass spectrum of complexes formed by Cu_n^+ clusters ($n = 4−7$) upon the reaction with H_2; energetics of 2H- vs H-loss; IR spectra for $[5Cu,2H/2D]^+$: ^{63}Cu vs ^{65}Cu; IR spectra of additional $[nCu, 2H]^+$ and $[nCu, 2D]^+$ ($n = 4−7$) local minima structures; H- and Cu-projected IR spectra of $[nCu, 2H]^+$ and $[nCu, 2D]^+$ ($n = 4−7$, equivalent to Figure 3a); similarity of $[nCu, 2H]^+$ and

[nCu, 2D]$^+$ (n = 4−7) modes (equivalent to Figure 3(b)); nudged elastic band calculations; IR spectra of Cu$_n^+$ clusters with two hydrogen molecules adsorbed (PDF)

AUTHOR INFORMATION

Corresponding Authors

Jörg Meyer − *Leiden Institute of Chemistry, Gorlaeus Laboratories, Leiden University, 2300 RA Leiden, The Netherlands;* ◉ orcid.org/0000-0003-0146-730X; Email: j.meyer@chem.leidenuniv.nl

Joost M. Bakker − *Radboud University, Institute for Molecules and Materials, FELIX Laboratory, 6525 ED Nijmegen, The Netherlands;* ◉ orcid.org/0000-0002-1394-7661; Email: J.Bakker@ru.nl

Authors

Olga V. Lushchikova − *Radboud University, Institute for Molecules and Materials, FELIX Laboratory, 6525 ED Nijmegen, The Netherlands;* ◉ orcid.org/0000-0002-5699-6818

Hossein Tahmasbi − *Leiden Institute of Chemistry, Gorlaeus Laboratories, Leiden University, 2300 RA Leiden, The Netherlands*

Stijn Reijmer − *Radboud University, Institute for Molecules and Materials, FELIX Laboratory, 6525 ED Nijmegen, The Netherlands*

Rik Platte − *Leiden Institute of Chemistry, Gorlaeus Laboratories, Leiden University, 2300 RA Leiden, The Netherlands*

Complete contact information is available at:
https://pubs.acs.org/10.1021/acs.jpca.0c11527

Notes

The authors declare no competing financial interest.

ACKNOWLEDGMENTS

REFERENCES

(1) van den Berg, A. W. C.; Areán, C. O. Materials for hydrogen storage: Current research trends and perspectives. *Chem. Commun.* 2008, 668−681.

(2) Behrens, M.; Studt, F.; Kasatkin, I.; Kühl, S.; Hävecker, M.; Abild-Pedersen, F.; Zander, S.; Girgsdies, F.; Kurr, P.; Kniep, B.-L.; et al. The active site of methanol synthesis over Cu/ZnO/Al$_2$O$_3$ industrial catalysts. *Science* 2012, 336, 893−897.

(3) Darling, G. R.; Holloway, S. Translation-to-vibrational excitation in the dissociative adsorption of D$_2$. *J. Chem. Phys.* 1992, 97, 734−736.

(4) Anger, G.; Winkler, A.; Rendulic, K. Adsorption and desorption kinetics in the systems H$_2$/Cu(111), H$_2$/Cu(110) and H$_2$/Cu(100). *Surf. Sci.* 1989, 220, 1−17.

(5) Berger, H. F.; Rendulic, K. D. An investigation of vibrationally assisted adsorption: the cases H$_2$/Cu(110) and H$_2$/Al(110). *Surf. Sci.* 1991, 253, 325−333.

(6) Sementa, L.; Wijzenbroek, M.; van Kolck, B. J.; Somers, M. F.; Al-Halabi, A.; Busnengo, H. F.; Olsen, R. A.; Kroes, G. J.; Rutkowski, M.; Thewes, C.; et al. Reactive scattering of H$_2$ from Cu(100):

Comparison of dynamics calculations based on the specific reaction parameter approach to density functional theory with experiment. *J. Chem. Phys.* 2013, 138, No. 044708.

(7) Madhavan, P.; Whitten, J. L. Theoretical studies of the chemisorption of hydrogen on copper. *J. Chem. Phys.* 1982, 77, 2673−2683.

(8) Hammer, B.; Scheffler, M.; Jacobsen, K. W.; Nørskov, J. K. Multidimensional Potential Energy Surface for H$_2$ Dissociation over Cu(111). *Phys. Rev. Lett.* 1994, 73, 1400−1403.

(9) White, J. A.; Bird, D. M.; Payne, M. C.; Stich, I. Surface Corrugation in the Dissociative Adsorption of H$_2$ on Cu(100). *Phys. Rev. Lett.* 1994, 73, 1404−1407.

(10) Diaz, C.; Pijper, E.; Olsen, R. A.; Busnengo, H. F.; Auerbach, D. J.; Kroes, G. J. Chemically Accurate Simulation of a Prototypical Surface Reaction: H$_2$ Dissociation on Cu(111). *Science* 2009, 326, 832−834.

(11) Doblhoff-Dier, K.; Meyer, J.; Hoggan, P. E.; Kroes, G.-J. Quantum Monte Carlo Calculations on a Benchmark Molecule-Metal Surface Reaction: H$_2$ + Cu(111). *J. Chem. Theory Comput.* 2017, 13, 3208−3219.

(12) Spiering, P.; Meyer, J. Testing Electronic Friction Models: Vibrational De-Excitation in Scattering of H$_2$ and D$_2$ from Cu(111). *J. Phys. Chem. Lett.* 2018, 9, 1803−1808.

(13) Geusic, M. E.; Morse, M. D.; Smalley, R. E. Hydrogen chemisorption on transition metal clusters. *J. Chem. Phys.* 1985, 82, 590−591.

(14) Morse, M. D.; Geusic, M. E.; Heath, J. R.; Smalley, R. E. Surface reactions of metal clusters. II. Reactivity surveys with D$_2$, N$_2$, and CO. *J. Chem. Phys.* 1985, 83, 2293−2304.

(15) Andersson, M.; Persson, J. L.; Rosén, A. Reactivity of Fe$_n$, Co$_n$, and Cu$_n$ clusters with O$_2$ and D$_2$ studied at single-collision conditions. *J. Phys. Chem. A* 1996, 100, 12222−12234.

(16) Kemper, P. R.; Weis, P.; Bowers, M. T.; Maître, P. Origin of Bonding Interactions in Cu$^+$ (H$_2$)$_n$ Clusters: An Experimental and Theoretical Investigation. *J. Am. Chem. Soc.* 1998, 120, 13494−13502.

(17) Manard, M. J.; Bushnell, J. E.; Bernstein, S. L.; Bowers, M. T. Origin of bonding interactions in Cu$_2^+$(H$_2$)$_n$ clusters: An experimental and theoretical investigation. *J. Phys. Chem. A* 2002, 106, 10027−10032.

(18) Rantala, T. T.; Nieminen, R. M. Cluster calculations for H$_2$ dissociation on Cu and Ni. *Phys. Scr.* 1988, 37, 141−144.

(19) Triguero, L.; Wahlgren, U.; Boussard, P.; Siegbahn, P. Calculations of hydrogen chemisorption energies on optimized copper clusters. *Chem. Phys. Lett.* 1995, 237, 550−559.

(20) Guvelioglu, G. H.; Ma, P.; He, X.; Forrey, R. C.; Cheng, H. Evolution of Small Copper Clusters and Dissociative Chemisorption of Hydrogen. *Phys. Rev. Lett.* 2005, 94, No. 026103.

(21) Guvelioglu, G. H.; Ma, P.; He, X.; Forrey, R. C.; Cheng, H. First principles studies on the growth of small Cu clusters and the dissociative chemisorption of H$_2$. *Phys. Rev. B* 2006, 73, No. 155436.

(22) Forrey, R. C.; Guvelioglu, G. H.; Ma, P.; He, X.; Cheng, H. Rate constants for dissociative chemisorption of hydrogen molecules on copper clusters. *Phys. Rev. B* 2006, 73, No. 155437.

(23) Kuang, X.-J.; Wang, X. Q.; Liu, G. B. A density functional study on the adsorption of hydrogen molecule onto small copper clusters. *J. Chem. Sci.* 2011, 123, 743−754.

(24) Hoyt, R. A.; Montemore, M. M.; Kaxiras, E. Nonadiabatic Hydrogen Dissociation on Copper Nanoclusters. *J. Phys. Chem. Lett.* 2018, 9, 5339−5343.

(25) López, N.; Illas, F.; Pacchioni, G. Electronic Effects in the Activation of Supported Metal Clusters: Density Functional Theory Study of H$_2$ Dissociation on Cu/SiO$_2$. *J. Phys. Chem. B* 1999, 103, 8552−8557.

(26) Lopez, N.; Illas, F.; Pacchioni, G. Ab initio theory of metal deposition on SiO$_2$. 1. Cu$_n$ (n = 1-5) clusters on nonbridging oxygen defects. *J. Phys. Chem. B* 1999, 103, 1712−1718.

(27) Lushchikova, O. V.; Huitema, D. M. M.; López-Tarifa, P.; Visscher, L.; Jamshidi, Z.; Bakker, J. M. Structures of Cu$_n^+$ (n = 3-10)

Clusters Obtained by Infrared Action Spectroscopy. *J. Phys. Chem. Lett.* **2019**, *10*, 2151−2155.

(28) Fielicke, A.; Kirilyuk, A.; Ratsch, C.; Behler, J.; Scheffler, M.; von Helden, G.; Meijer, G. Structure determination of isolated metal clusters via far-infrared spectroscopy. *Phys. Rev. Lett.* **2004**, *93*, No. 023401.

(29) Swart, I.; Gruene, P.; Fielicke, A.; Meijer, G.; Weckhuysen, B. M.; de Groot, F. M. F. Molecular adsorption of H_2 on small cationic nickel clusters. *Phys. Chem. Chem. Phys.* **2008**, *10*, 5743−5745.

(30) Swart, I.; de Groot, F. M.; Weckhuysen, B. M.; Gruene, P.; Meijer, G.; Fielicke, A. H_2 adsorption on 3d transition metal clusters: A combined infrared spectroscopy and density functional study. *J. Phys. Chem. A* **2008**, *112*, 1139−1149.

(31) Vanbuel, J.; Fernández, E. M.; Ferrari, P.; Gewinner, S.; Schöllkopf, W.; Balbás, L. C.; Fielicke, A.; Janssens, E. Hydrogen Chemisorption on Singly Vanadium-Doped Aluminum Clusters. *Chem. - Eur. J.* **2017**, *23*, 15638−15643.

(32) Jia, M.; Vanbuel, J.; Ferrari, P.; Fernández, E. M.; Gewinner, S.; Schöllkopf, W.; Nguyen, M. T.; Fielicke, A.; Janssens, E. Size Dependent H_2 Adsorption on Al_nRh^+ (n = 1-12) Clusters. *J. Phys. Chem. C* **2018**, *122*, 18247−18255.

(33) Bakker, J. M.; Lapoutre, V. J. F.; Redlich, B.; Oomens, J.; Sartakov, B. G.; Fielicke, A.; von Helden, G.; Meijer, G.; van der Meer, A. F. G. Intensity-resolved IR multiple photon ionization and fragmentation of C_{60}. *J. Chem. Phys.* **2010**, *132*, No. 074305.

(34) Haertelt, M.; Lapoutre, V. J. F.; Bakker, J. M.; Redlich, B.; Harding, D. J.; Fielicke, A.; Meijer, G. Structure Determination of Anionic Metal Clusters via Infrared Resonance Enhanced Multiple Photon Electron Detachment Spectroscopy. *J. Phys. Chem. Lett.* **2011**, *2*, 1720−1724.

(35) Dietz, T. G.; Duncan, M. A.; Powers, D. E.; Smalley, R. E. Laser production of supersonic metal cluster beams. *J. Chem. Phys.* **1981**, *74*, 6511−6512.

(36) Goedecker, S. Minima hopping: An efficient search method for the global minimum of the potential energy surface of complex molecular systems. *J. Chem. Phys.* **2004**, *120*, 9911−9917.

(37) Bao, K.; Goedecker, S.; Koga, K.; Lançon, F.; Neelov, A. Structure of large gold clusters obtained by global optimization using the minima hopping method. *Phys. Rev. B* **2009**, *79*, No. 041405.

(38) Rasoulkhani, R.; Tahmasbi, H.; Ghasemi, S. A.; Faraji, S.; Rostami, S.; Amsler, M. Energy landscape of ZnO clusters and low-density polymorphs. *Phys. Rev. B* **2017**, *96*, No. 064108.

(39) Larsen, A. H.; Mortensen, J. J.; Blomqvist, J.; Castelli, I. E.; Christensen, R.; Dułak, M.; Friis, J.; Groves, M. N.; Hammer, B.; Hargus, C.; et al. The atomic simulation environment—a Python library for working with atoms. *J. Phys.: Condens. Matter* **2017**, *29*, No. 273002.

(40) Blum, V.; Gehrke, R.; Hanke, F.; Havu, P.; Havu, V.; Ren, X.; Reuter, K.; Scheffler, M. Ab initio molecular simulations with numeric atom-centered orbitals. *Comput. Phys. Commun.* **2009**, *180*, 2175−2196.

(41) Perdew, J. P.; Burke, K.; Ernzerhof, M. Generalized Gradient Approximation Made Simple. *Phys. Rev. Lett* **1996**, *77*, 3865−3868.

(42) Behler, J. Atom-centered symmetry functions for constructing high-dimensional neural network potentials. *J. Chem. Phys.* **2011**, *134*, No. 074106.

(43) Amsler, M.; Rostami, S.; Tahmasbi, H.; Khajehpasha, E. R.; Faraji, S.; Rasoulkhani, R.; Ghasemi, S. A. FLAME: A library of atomistic modeling environments. *Comput. Phys. Commun.* **2020**, *256*, No. 107415.

(44) Perdew, J. P.; Ernzerhof, M.; Burke, K. Rationale for mixing exact exchange with density functional approximations. *J. Chem. Phys.* **1996**, *105*, 9982−9985.

(45) Adamo, C.; Barone, V. Toward reliable density functional methods without adjustable parameters: The PBE0 model. *J. Chem. Phys.* **1999**, *110*, 6158−6170.

(46) Porezag, D.; Pederson, M. R. Infrared Intensities and Raman-Scattering Activities within Density-Functional Theory. *Phys. Rev. B* **1996**, *54*, 7830−7836.

(47) Tang, W.; Sanville, E.; Henkelman, G. A Grid-Based Bader Analysis Algorithm without Lattice Bias. *J. Phys.: Condens. Matter* **2009**, *21*, No. 084204.

(48) Henkelman, G.; Uberuaga, B. P.; Jónsson, H. A climbing image nudged elastic band method for finding saddle points and minimum energy paths. *J. Chem. Phys.* **2000**, *113*, 9901−9904.

(49) Oomens, J.; Sartakov, B. G.; Meijer, G.; von Helden, G. Gas-phase infrared multiple photon dissociation spectroscopy of mass-selected molecular ions. *Int. J. Mass Spectrom.* **2006**, *254*, 1−19.

(50) López-Caballero, P.; Hauser, A. W.; Pilar de Lara-Castells, M. Exploring the Catalytic Properties of Unsupported and TiO_2-Supported Cu_5 Clusters: CO_2 Decomposition to CO and CO_2 Photoactivation. *J. Phys. Chem. C* **2019**, *123*, 23064−23074.

(51) Claes, P.; Janssens, E.; Ngan, V. T.; Gruene, P.; Lyon, J. T.; Harding, D. J.; Fielicke, A.; Nguyen, M. T.; Lievens, P. Structural Identification of Caged Vanadium Doped Silicon Clusters. *Phys. Rev. Lett.* **2011**, *107*, No. 173401.

(52) Guo, H.; Sautet, P.; Alexandrova, A. N. Reagent-Triggered Isomerization of Fluxional Cluster Catalyst via Dynamic Coupling. *J. Phys. Chem. Lett.* **2020**, *11*, 3089−3094.

(53) Solans-Monfort, X.; Branchadell, V.; Sodupe, M.; Zicovich-Wilson, C. M.; Gribov, E.; Spoto, G.; Busco, C.; Ugliengo, P. Can Cu^+-Exchanged Zeolites Store Molecular Hydrogen? An Ab-Initio Periodic Study Compared with Low-Temperature FTIR. *J. Phys. Chem. B* **2004**, *108*, 8278−8286.

(54) Veccham, S. P.; Head-Gordon, M. Density Functionals for Hydrogen Storage: Defining the H2Bind275 Test Set with Ab Initio Benchmarks and Assessment of 55 Functionals. *J. Chem. Theory Comput.* **2020**, *16*, 4963−4982.

(55) Haertelt, M.; Lyon, J. T.; Claes, P.; de Haeck, J.; Lievens, P.; Fielicke, A. Gas-phase structures of neutral silicon clusters. *J. Chem. Phys.* **2012**, *136*, No. 064301.